PCCP

Accepted Manuscript

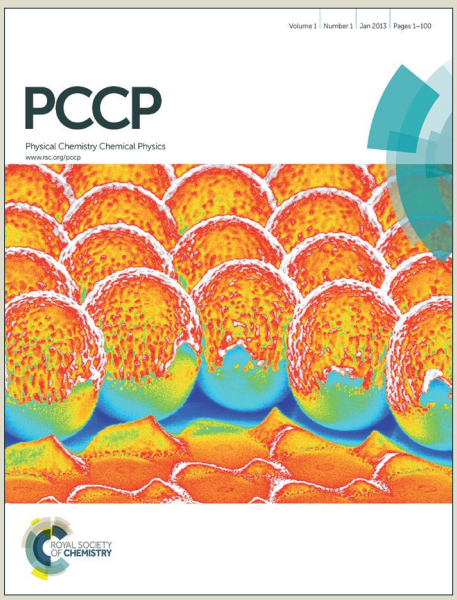

ROYAL SOCIETY OF CHEMISTRY

www.rsc.org/pccp

A global full-dimensional potential energy surface and quasiclassical trajectory study of the $O(^1D)+CH_4$ multichannel reaction

Kejie Shao, Bina Fu[a], Dong H. Zhang[a]

State Key Laboratory of Molecular Reaction Dynamics and Center for Theoretical and Computational Chemistry, Dalian Institute of Chemical Physics, Chinese Academy of Sciences, Dalian, P.R. China 116023

(Dated: August 6, 2015)

Abstract

We report a new global, full-dimensional ground-state potential energy surface (PES) of the $O(^1D) + CH_4$ multichannel reaction, based on high-level *ab initio* calculations and fitting procedures. The PES is a permutationally invariant fit to roughly 340 000 electronic energies calculated by MRCI+Q/aug-cc-pVTZ level of theory. Extensive quasiclassical trajectory calculations were carried out on the new PES at the collision energy of relevance to the previously universal crossed molecular beam experiments. The product branching ratios, translational energy distributions and angular distributions of $OH+CH_3$, $H+CH_2OH/CH_3O$ and H_2+HCOH/H_2CO product channels were calculated and compared with the available experimental results. Very good agreement between theory and experiment has been achieved. The $O(^1D) + CH_4$ reaction mainly proceeds through the CH_3OH intermediate via the trapped abstraction mechanism, starting with the abstraction of the hydrogen atom, rather than the direct insertion pathway with the $O(^1D)$ atom directly inserting into the C-H bond of CH_4. The process with a very short lifetime behaves like an abstraction reaction, producing a pronounced forward scattering peak as found in the $OH+CH_3$ channel, while the process with a relatively long lifetime produces reaction products with nearly forward and backward scattering symmetry, similar to an insertion reaction, as found in other reaction channels.

[a] Authors to whom correspondence should be addressed. Electronic addresses: bina@dicp.ac.cn and zhangdh@dicp.ac.cn

PACS numbers:

I. INTRODUCTION

Experimental and theoretical studies on polyatomic reactions have extended and greatly advanced our understanding of chemical reaction dynamics over the last decade[1–14]. Methane is the simplest alkane and the most abundant hydrocarbon in the atmosphere. The reactions of methane with H/F/Cl/O(^3P) atoms, which are known as direct abstraction/exchange reactions, have been extensively studied[1–10, 15, 16], for which many interesting dynamical features have been observed. Despite significant progress made in past decades, it is still challenging to elucidate dynamics mechanisms for polyatomic reactions, in particular, involving complex formation, in which a reaction intermediate exists. Such an intermediate is formed due to a potential well along the reaction path, which eventually breaks apart to form the product species. Different from the O(^3P) atom, the reactions of O(^1D) with some gas phase molecules, such as NH_3, CH_4, C_2H_6 and C_3H_8, are complex-forming reactions[17–22], with deep wells on the ground-state potential energy surfaces(PESs).

Due to its significance in both the atmospheric and combustion chemistry, the reaction of O(^{1}D) with methane has attracted great attention both experimentally and theoretically[14, 18, 19, 23–33]. It has been long regarded as a prototype of polyatomic insertion reaction, in which the O(^{1}D) atom can is thought to directly insert into the C-H bond of methane. Extensive experimental and theoretical studies have been carried out to unravel the dynamics of this typical multichannel polyatomic complex-forming reaction, posing challenges for theory and experiments owing to the ruggedness and high dimensionality of this potential.

In 2000, Yang and co-workers investigated the O(^1D) + CH_4 reaction using the universal crossed molecular beam technique[18], indicating OH+CH_3 is the main reaction channel, with its branching percentage of roughly 77%, whereas H and H_2 elimination channels are minor processes. Product translational energy and angular distributions were determined for the observed reaction channels, indicating the products of the H atom formation channel are slightly backward scattered, and those of the H_2 formation channel show an isotropic angular distribution. The angular distribution of the OH product shows both forward and backward peaks, with the forward scattering peak remarkably higher than the backward peak. This is probably not consistent with the direct insertion reaction picture, which is more likely to exhibit forward backward scattering symmetry[34, 35].

Recent experimental studies were focused on the OH/OD product channel for the $O(^1D)$ + CH_4/CD_4 reaction, but not for the H or H_2 product channels. Specifically, Suzuki and co-workers carried out crossed molecular beam ion imaging experiment on the $O(^1D)$ + $CD_4/CH_4 \rightarrow OD/OH + CD_3/CH_3$ reaction[24–26]. Two distinctive reaction mechanisms were observed, in which the supposed "insertion" reaction on the ground-state PES exhibits a strongly forward scattering angular distribution, whereas the abstraction channel shows a clear backward scattering angular distribution with discrete structures and occurs most likely on the excited-state PES, as suggested by Hernando *et al*[30]. More recently, a time-sliced velocity map imaging crossed beams experiment on the $O(^1D) + CD_4 \rightarrow OD + CD_3$ reaction was performed by Yang and co-workers, showing that the abstraction pathway is a minor process[27, 28], consistent with Suzuki's recent experimental results[25].

Theoretically, the stationary points on the ground-state PES of the $O(^1D) + CH_4$ reaction were characterized, and a direct-dynamics study of this reaction was performed by Yu and Muckerman[32]. However, due to the large computational effort this approach entails, a low-level electronic structure method was used and limited trajectories were propagated for a short time. A clear dynamical picture for the ground-state reaction was not obtained.

In light of the vast and valuable information accumulated for the $O(^1D)$ reaction with CH_4 and its isotopes, a comprehensive theoretical investigation based on first principles, which can provide direct comparison with the experimental results and would subsequently shed light on this intriguing and yet not fully comprehended reaction mechanism is highly desirable. Very recently, we reported a joint experimental and theoretical study on the $O(^1D)$ + $CHD_3 \rightarrow OH + CD_3$ reaction[14]. Unprecedented details have been unraveled for the dynamics of this reaction with comprehensive quasiclassical trajectory (QCT) calculations, based on an accurate, full-dimensional *ab initio* PES, which were able to produce dynamics results in good agreement with the time-sliced velocity map imaging experiment at the collision energy (E_c) of 6.8 kcal/mol. Furthermore, we found that this reaction proceeds with the initial abstraction of H atom by $O(^1D)$ from CHD_3, rather than the direct insertion of $O(^1D)$ atom into the C-H bond of CHD_3, forming an extremely short-lived or long-lived CD_3OH complex before its decomposition. This mechanism is similar with the process first observed in the triatomic reaction $O(^1D)$+HCl/HF $\rightarrow$ OH+Cl/F[36, 37], in which the $O(^1D)$ atom initially attaches to the H atom, instead of inserting into the Cl-H bond, although a genuine insertion does occur at low impact parameters. We termed this reaction mechanism

"trapped abstraction", for which the formation of extremely short-lived intermediate is responsible to the predominantly forward scattering angular distribution of CD_3 relative to the incoming CHD_3[14].

In this article, we present the details of the ground-state PES of the $O(^1D)$+CH_4 multi-channel reaction, and QCT calculations on this PES. In addition to the OH+CH_3 formation channel, the dynamical details of H+CH_3O/CH_2OH and H_2+HCOH/H_2CO were also investigated, and compared with the results of the universal crossed molecular beam experiment performed by Yang and co-workers in 2000[18].

The paper is organized as follows. In Sec. II, we present the construction details and properties of the PES, together with QCT calculations. Section III gives the dynamics features obtained by the QCT calculations on the new PES. A summary of the current results and conclusions are given in Sec. IV.

II. POTENTIAL ENERGY SURFACE AND QUASICLASSICAL TRAJECTORY CALCULATIONS

$O(^1D)$ has a five-fold degenerate electronic state, and its interactions with methane creates one ground-state and four excited-state potential energy surfaces. Note that the first excited state is also correlated with OH + CH_3, however, it is ignored in the current theory due to its small contributions to the overall reactivity at low collision energies[14, 27]. We constructed a new ground-state PES of the $O(^1D)$ + CH_4 reaction based on high-level *ab initio* and fitting methods. Specifically, a total of roughly 340 000 *ab initio* points were calculated and included in the permutationally invariant polynomial fitting procedure[38, 39]. These electronic structure calculations were done by the multiconfiguration reference internally contracted configuration interaction with Davidson correction (MRCI+Q) method using the MOLPRO suite of codes[40]. The orbitals for the MRCI+Q calculations were taken from six-state complete-active-space self-consistent field (CASSCF) calculations using the dynamical weighting (DW) for each state. The DW-CASSCF calculations with a $sech^2$ weighting function(β^{-1}=3 eV) have been performed[41]. As we constructed the PES with the total energy up to 70 kcal/mol above the $O(^1D)$+CH_4 asymptote, including the sixth state is useful in optimizing the orbitals in the high energy regions. The active space used in both the CASSCF and MRCI+Q calculations was 18 electrons in 10 orbitals. The calculations

with full-valence space with 14 electrons in 12 orbitals are ideal, but they are extremely expensive to develop a global PES for the title reaction when 340 000 energy points were computed. Lots of tests were performed by us using different active spaces, and the current active space was chosen because this wave function can smoothly connect the large regions of the PES of interest.

The energy points used in the fitting were selected properly based on direct dynamics simulations and further QCT calculations using the preliminary PESs. The initial data set consists of roughly 40,000 electronic energies with the configurations taken from direct dynamics calculations using the unrestricted B3LYP/6-31+g* level of theory. For these calculations, a total of about 400 trajectories were run from the reagents $O(^1D)$+CH_4 at the collision energies of 6.8 kcal/mol and 10.0 kcal/mol, respectively. Additional roughly 400 trajectories were run initiated from the various transition state (TS) regions leading to different product channels. Starting from the first PES based on the initial $\sim$ 40,000 MRCI+Q/aug-cc-pVTZ energies, more data points were added iteratively by doing QCT calculations on those preliminary PESs. Further nuclear configurations for the database in the complex regions were obtained by random displacement of Cartesian coordinates about stationary points. In addition, more data points around the reaction pathways leading to different product channels were computed and added to the data set.

The fit used a basis of permutationally invariant polynomials of Morse-like variables in all internuclear distances [$y_{ij} = \exp(-r_{ij}/\lambda)$; where $\lambda = 2.0$ bohrs]. Then the PES is represented in terms of all 15 such variables, by[38, 39]

$$V = \sum_{m=0}^{M} C_{n_1 n_2 \cdots n_{14} n_{15}} S(y_{12}^{n_1} y_{13}^{n_2} y_{14}^{n_3} \cdots y_{46}^{n_{14}} y_{56}^{n_{15}}), \quad (1)$$

where S is a "symmetrization" operator, and where $C_{n_1 n_2 \cdots n_{14} n_{15}}$ are the unknown linear coefficients, which are determined by standard linear least-squares fitting to all the data. In this fit, the total order of polynomials involved in the expression ($M = n_1+n_2+n_3+\cdots n_{14}+n_{15}$) does not exceed eight (a total of 9355 terms). The RMS error of the fitted surface is 1.0 kcal/mol for energies up to 230 kcal/mol relative to the global minimum (methanol) of the PES. The final PES is well converged with respect to the fitting errors and dynamics features. The PES is available from the corresponding authors upon request.

Figure 1 shows a complete schematic of the ground-state PES, including the stationary-

point structures and energies relative to the reagents $O(^1D)+CH_4$ (with vibrational zero-point energies not included). As seen, there are several saddle points and product channels, together with one global minimum on the PES. Due to the complexity of the PES for this system, the fitting is challenging to describe accurately all of the stationary points and reaction channels. The corresponding relative energies to the reagent, vibrational zero-point energies(ZPEs) and harmonic frequencies of stationary points obtained on the PES are shown in Table I. The comparisons made for the energies obtained from the current PES and MRCI+Q/AVTZ calculations show very good agreement among them, as shown in Fig. 1 and Table I. The harmonic frequencies from theory are also compared with available experimental results[42].

The reaction paths for various product channels, which were determined by the Quadratic Steepest Descent method[43] on the PES, were displayed in Fig. 2, together with those results calculated by MRCI+Q/AVTZ level of theory. We see very smooth reaction path curves from the PES for different channels. Furthermore, excellent agreement for energies on the reaction paths is achieved between the PES and MRCI+Q/AVTZ values. The maximum fitting error for energy points on the reaction paths is only 0.4 kcal/mol.

A comparison is also made for the theoretical energetics of products (ZPEs included) and available experimental values[44] relative to $O(^1D) + CH_4$ in Table II. The agreement between theory and experiment is satisfactory, with the largest deviation of 3.8 kcal/mol for the H_2+H_2CO channel, which is located roughly 115 kcal/mol below the reagent.

The CH_3OH intermediate is located at 132.3 kcal/mol (ZPE included) below the $O(^1D) + CH_4$ asymptote, resulting in a very deep well along the reaction path. The $O(^1D)+CH_4$ reaction can, in principle, evolve via this deep well on the PES and subsequently decompose to various products. There are seven possible reaction pathways on the PES, starting at the CH_3OH intermediate, with the formation of $OH+CH_3$ and two H elimination channels $H+CH_3OH/CH_2OH$ without a barrier, three H_2 elimination channels H_2+H_2CO/trans-HCOH/cis-HCOH via TS1, *trans*-TS2, *cis*-TS2, respectively, and the formation of H_2O+CH_2 via TS3.

Standard QCT calculations[45, 46] for the title reaction were carried out at the collision energy (E_c) of 6.8 kcal/mol (the collision energy of the crossed molecular beam experiment) on the newly constructed PES with CH_4 initially in the ground rovibrational state. Initial coordinates and momenta of CH_4 were obtained by randomly sampling the normal coordi-

nates and momenta. Adjustments were then made to the momenta to enforce zero angular momentum of CH_4. The initial distance of the $O(^1D)$ atom from the center of mass of CH_4 was $\sqrt{x^2+b^2}$, where b is the impact parameter and x was set to 11.0 bohrs. The maximum impact parameter (b_{max}) was set to 7.5 bohrs. The orientation of CH_4 was randomly sampled and b was selected randomly from the distribution $b_{max}\sqrt{r}$, where r is a random number uniformly distributed from 0 to 1. Roughly 8,000,000 trajectories were run using the velocity-Verlet integration algorithm with a time step of 0.073 fs for a maximum time of 100 ps. The trajectories were terminated when the distance of two fragments became larger than 12 bohrs. Almost all trajectories conserved energy to within 0.05 kcal/mol, confirming the smoothness and accuracy of the PES. We found the trajectories ended up going into various product channels or returning to the reactants using the maximum propagation time we set. The ZPE constraint results[12, 13, 47], obtained from those trajectories in which each product has at least the corresponding ZPE are given.

III. RESULTS AND DISCUSSIONS

One of the most useful pieces of information desirable on the dynamics of a multichannel reaction is the branching ration of the various channels. By analyzing all the trajectories, we get the relative branching percentages at E_c=6.8 kcal/mol of the seven product channels as follows.

$$\begin{aligned}
O(^1D) + CH_4 &\rightarrow OH + CH_3 && (80.1\%)\\
&\rightarrow H + CH_2OH && (9.7\%)\\
&\rightarrow H + CH_3O && (1.9\%)\\
&\rightarrow H_2 + H_2CO && (1.2\%)\\
&\rightarrow H_2 + \textit{trans}\text{-HCOH} && (1.4\%)\\
&\rightarrow H_2 + \textit{cis}\text{-HCOH} && (0.8\%)\\
&\rightarrow H_2O + CH_2 && (4.9\%)
\end{aligned}$$

We note that the H_2O channel can not be detected in the universal crossed molecular beam experiment due to the low resolution at that time[18], although its theoretical yield accounts for 4.9%. In addition, various product isomers can not be identified by experiment. The primary product branching ratios obtained by theory and experiment[18] are shown in

Table III. In Table III the H_2O channel is not included in the accounting of the percentages to be consistent with experiment. The branching percentages of OH, H and H_2 channels obtained by theory are 84.2%, 12.2% and 3.6%, in good agreement with the experimental results of 77%, 18% and 5%, respectively, indicating OH+CH_3 is the dominant reaction pathway.

A. The OH+CH_3 channel

This channel accounts for roughly 80% of the total product yield in the O(^{1}D)+CH_4 multichannl reaction, obtained both from theory and experiment. The center of mass (CM) translational energy distribution of OH+CH_3, and angular distribution of CH_3 obtained by the QCT calculations on the newly constructed PES are displayed in Fig. 3(a) and Fig. 3(b), respectively. The behavior of the translational energy distribution, P(E_T), supports that the pathway leading to CH_3+OH on the ground-state PES is barrierless, with the P(E_T) that peaks at around 7 kcal/mol with a long tail up to the energy of about 44.0 kcal/mol. The averaged translational energy release for this channel is about 11.0 kcal/mol, corresponding to a small fraction (0.25) of the total available energy ($\sim$ 44 kcal/mol), and this agrees well with the experimental measurement[18] of 12.0 kcal/mol, indicating that most of the available energy in this channel is deposited into the internal degrees of freedom of the molecular radical products.

The resulting rovibrational state distributions of OH are shown in Fig. 4. We can see considerable vibrational excitations of OH, with the vibrational populations up to v=4. As shown in Fig. 4(b), the peak of the rotational distributions of OH in different vibrational states gradually changes from N=15 for v=0 to N=8 for v=4. We have also calculated mode-specific $CH_3(n_1n_2n_3n_4)$ vibrational distributions to further investigate the CH_3+OH product channel. The corresponding frequencies for each mode of CH_3 are given in Table I. The normal-mode analysis of CH_3 based on the total vibrational energy of the vibrational states were done using the same approach as described in elsewhere[48, 49]. Figure 5(a) shows the mode-specific vibrational distributions of CH_3, indicating CH_3 vibrational state is highly excited, especially for the umbrella bending (ω_1) and scissor bending (ω_2) modes. All the vibrational states shown here correspond to about 34.2% of the total CH_3 vibrational populations, implying many higher excited states are open as well, though their respective

population is relatively small. The largest population is on the ground state, but it only accounts for about 6% of the total populations, compared to 4% and 4.5% respectively, for the states (1000) and (0100). A rather broad distribution is shown for the umbrella bending overtone, with considerable populations for the quantum number up to 6. The excitation of the symmetric stretching ω_3 and asymmetric stretching ω_4 is also seen, with the $CH_3(\omega_3{=}1)$ and $CH_3(\omega_4{=}1)$ populations roughly 2 times smaller than the ground state of CH_3. A broad distribution for the rotational states of CH_3 is seen in Fig. 5(b), with its peak at roughly j=7 and its distribution up to j=40.

The angular distribution of the OH product in Fig. 3 (b) shows a predominant forward scattering peak relative to the $O(^1D)$ beam direction, with a small backward scattering peak and relatively small signals from the sideways scattering. The behavior of this distribution is very similar to that of the recent calculations for the $O(^1D)+CHD_3 \rightarrow OH+CD_3$ reaction[14], which closely resembles the experimental results of $O(^1D)+CH_4 \rightarrow OH+CH_3$ by Yang and co-workers in 2000[18] with a pronounced forward peak and a relatively small backward one, despite the fact that the direct abstraction reaction proceeding on the excited-state PES, which can also produce backward scattering peak, is ignored in the current theory due to its small contributions to the overall reactivity. A 3D polar plot for the product translational energy and angular distributions for the $OH+CH_3$ channel is shown in Fig. 6. It is distinct that the predominant forward scattering peak mainly resides in the low kinetic energy region, indicating the high internal excitation of the products.

As has been speculated in early experiment[18], this dynamical picture is not consistent with the direct insertion mechanism as has long been thought, which is more likely to lead to the forward and backward scattering symmetry. The origin of the predominantly forward scattering as well as the backward and sideways scattering is unknown, until recently the true reaction mechanism for the reaction of $O(^1D)$ with isotopically substituted CHD_3 is elucidated by us, which we termed "trapped abstraction". By further investigating into the current QCT results, we found $O(^1D)+CH_4 \rightarrow OH+CH_3$ also mainly proceeds via the trapped abstraction mechanism, rather than the direct insertion mechanism. Specifically, the reaction initially takes place through the $O(^1D)$ abstraction of H atom out of CH_3, instead of inserting into the C-H bond. The consequently formed CH_3OH complex is easy to dissociate because the energy released from complex formation is highly localized in relative motion of OH and CH_3. As a result, more than half population of complex have short life time with

OH and CH_3 vibrating relatively only once, producing a pronounced forward scattering peak by stripping mechanism with initial large impact parameters and a backward scattering peak by rebounding mechanism with small impact parameters as observed for this reaction and its isotopes.

B. The H formation channel

As shown in Table III, the H formation channel accounts for more than 10% of the total product yield and can be considered as a second important channel. There are two H formation processes on the ground-state PES of the title reaction, i.e., H+CH_2OH and H+CH_3O, as shown in Fig. 1. As has been obtained from the QCT calculations, the relative branching percentage of H+CH_2OH is roughly 4 times larger than that of H+CH_3O, indicating H+CH_2OH is the dominant product for the H formation channel. However, the two H formation processes were not exactly identified by early experiment, and the results attribute to the sum of two contributions[18]. It is interesting that no large differences have been seen between these two H formation processes in the QCT calculations, for the resulting translational energy and angular distributions. Hence, we show the total translational energy and angular distributions of the sum of contributions from the two H formation processes in Fig. 7. The $P(E_T)$ peaks at about 6 kcal/mol and has an average amount of energy in translation of 9.5 kcal/mol, corresponding to a fraction of 26% as computed for the H+CH_2OH channel (the total available energy is roughly 36 kcal/mol for H+CH_2OH and 27 kcal/mol for H+CH_3O). This small fraction of energy in translation indicates most of the available energy is channeled into the internal excitations of CH_2OH. The overall behavior of the translational energy distribution is quite similar to that of the experimental results[18], which supports that the dynamics of this channel is barrierless.

As shown in Fig. 7(b), the angular distribution of the H formation channel behaves nearly symmetric with respect to the forward and backward directions, as expected for a long-time complex formation reaction. A 3D polar plot for the product translational energy and angular distributions for the H formation channel is shown in Fig. 8, indicating the forward and backward scattering signals are slightly stronger than those of the sideways scattering. From the experimental angular distribution, the radical product (CH_2OH/CH_3O) from the H formation channel is noticeably backward scattered with regard to the O(^{1}D)

beam direction. However, in the experimental 3D polar plot, the product only looks slightly backward scattered, which resembles that of the theoretical results showing almost forward and backward scattering symmetry. Detailed analysis of the trajectories shows that the two H formation processes mainly proceed through the CH_3OH intermediate, starting with the abstraction of the hydrogen atom, similar to the initial step in producing $OH+CH_3$. Only a very small portion ($< 1\%$) of trajectories goes through the typical direct insertion pathway, with the $O(^1D)$ atom directly inserting into the C-H bond of CH_3. However, different from the $OH+CH_3$ formation process, only the CH_3OH intermediate with a long lifetime produces $H+CH_2OH/CH_3O$, thus resulting in the forward and backward scattering symmetry, similar to an insertion reaction.

C. The H_2 formation channel

Another reaction channel the experiment observed is the H_2 formation, which accounts for 5% and 3.6% of the total reaction yield obtained from theory and experiment, respectively. As shown in Fig. 1, there are three H_2 formation pathways on the ground-state PES via the CH_3OH intermediate, which further decomposes to H_2+*cis*-HCOH, H_2+*trans*-HCOH and H_2+H_2CO, respectively. The *cis*-HCOH and *trans*-HCOH channels are produced via the similar barrier heights (differing by ~ 1 kcal/mol) starting from CH_3OH, with the reaction exothermicity differing by ~ 5 kcal/mol, while the H_2CO channel is formed through a higher barrier and with much more exothermicity. The relative branching ratio of H_2+HCOH (the sum of *cis*-HCOH and *trans*-HCOH) versus H_2+H_2CO is 65% : 35% obtained from the current theory, whereas the three isomers were not exactly identified by experiment[18]. Since the H_2+H_2CO channel has a much higher reverse barrier than the HCOH process, the former channel should be less favorable, which is verified by the current QCT results.

Figure 9 (a) displays the total translational energy distribution of the H_2 formation channel, together with the translational energy distributions of H_2+HCOH and H_2+H_2CO pathways, respectively. It is interesting that the total translational energy distribution demonstrates obviously the bimodal structure, with one peak at around 22 kcal/mol and one at roughly 60 kcal/mol, in accord with the experimental results[18]. Since H_2+HCOH and H_2+H_2CO formation processes are energetically significantly different from each other, it was presumed by experiment that the higher translational energy peak has to result from

the H_2+H_2CO channel and the lower peak in the product translational energy distribution probably comes from the H_2+HCOH channel, which has a much lower reverse reaction barrier. This is verified by the present QCT calculations on the new PES, which can also obtain each $P(E_T)$ curve for H_2+HCOH and H_2+H_2CO. As shown, the translational energy distribution of H_2+HCOH peaks at around 22 kcal/mol, and vanishes at the available energy of about 58 kcal/mol. The $P(E_T)$ distribution of H_2+H_2CO behaves differently, with a peak at around 60 kcal/mol, reaching up to the total available energy of about 110 kcal/mol. The overall behavior of the translational energy distributions of H_2+HCOH and H_2+H_2CO supports that the dynamics of the two channels is dominated by the exit channel barrier, which is quite different from that of H+CH_2OH/CH_3O or OH+CH_3.

The isotropic angular distribution of the H_2 formation channel shown in Fig. 9(b) agrees well the experimental results[18], with the forward scattering signal slightly stronger than the backward scattering. The 3D polar plot for the translational energy distribution and angular distribution of the H_2 formation channel is much more complicated, as we see from Fig. 10. The H_2CO product should be clearly faster than HCOH due to the remarkably different exothermicity and translational energy distributions, thus the outer-sphere distribution with larger velocity arises from the H_2CO channel, whereas the inner-sphere distribution with smaller velocity results from the HCOH channel. Both the two H formation channels yield products with isotropic angular distributions. By investigating the trajectories for the two channels, we find a long-lived intermediate CH_3OH is formed before its decomposition into H_2+HCOH/H_2CO, similar to the H formation channel. Furthermore, the complex is nearly exclusively formed by the abstraction of H atom from CH_4 by $O(^1D)$, followed by sliding into the deep CH_3OH well , but not by the direction insertion of $O(^1D)$ into the C-H bond of CH_4.

To investigate the lifetime differences among the OH formation, H formation and H_2 formation channels, we calculated the distributions of times for these reaction channels, defined as the duration time for a reactive trajectory proceeding from the reactant side to product side with a distance between two fragments of 6 bohrs. As shown in Fig. 11, the reaction time distribution for OH+CH_3 is quite similar to OH+CD_3 as we discussed for the $O(^1D)$+CHD_3 $\rightarrow$ OH+CD_3 reaction[14], which is noticeably peaked at around 150 fs, with a long but small tail up to several picoseconds. The predominantly forward scattering for this channel arises from the very short reaction time. In contrast, the products for H and

H_2 formation channels are dominantly contributed from the CH_3OH intermediate with long lifetime (¿500 fs), although a small portion of products also comes from trajectories with relatively short reaction time. As a result, the H and H_2 formation channels result in nearly forward and backward scattering symmetry and isotropic angular distribution.

IV. CONCLUSIONS

To summarize, a new *ab initio* global PES of the $O(^1D)+CH_4$ multichannel reaction is calculated in this study. The PES is constructed by fitting roughly 340 000 MRCI+Q/aug-cc-pVTZ calculations of electronic energies, using permutationally invariant polynomials. Extensive QCT calculations have been performed on the fitted PES, and detailed dynamics information of the $OH+CH_3$, $H+CH_2OH/CH_3O$ and H_2+HCOH/H_2CO product channels are presented and compared with the available experimental results. Good agreement between the QCT calculations and experiment has been achieved for the product branching ratios, translational energy distributions and angular distributions. The product branching percentages of OH, H and H_2 channels obtained by theory are 84.2%, 12.2% and 3.6%, in good agreement with the experimental results of 77%, 18% and 5%, respectively, indicating $OH+CH_3$ is the dominant reaction pathway. The angular distribution of OH displays a predominantly forward scattering peak, with a small backward scattering peak, while the products of the H atom formation channel show nearly forward scattering and backward scattering symmetry, and the products of the H_2 formation process show an isotropic angular distribution.

Further investigations of the trajectories shows the $O(^1D)+CH_4$ reaction mainly proceeds through the CH_3OH intermediate via the trapped abstraction mechanism[14], starting with the abstraction of the H atom from CH_4 by $O(^1D)$, with only a very small portion of trajectories going through the typical direct insertion pathway with the $O(^1D)$ atom directly inserting into the C-H bond of CH_4. The trajectories with short lifetimes behave as an abstraction reaction, mainly producing backward-scattered product with initial small impact parameters and forward-scattered product with large impact parameters, as has been found in most reactive trajectories of the $OH+CH_3$ channel and thus resulting in the dominantly forward scattering of this channel.

A significant portion of trajectories are trapped in the CH_3OH well for a long period of

time, although they also start with the abstraction of the H atom. These kinds of trajectories manifest as those for an insertion barrierless reaction, producing products with forward and backward symmetry, as found in all the reactive trajectories of the H+CH_2OH/CH_3O channel and some reactive trajectories of the OH+CH_3 channel. The reaction mechanism of the H_2 formation channel is similar to the H formation channel, except that the dynamics of H_2+HCOH/H_2CO is dominated by the exit channel barrier.

We anticipate that this reaction mechanism should also be responsible for the reaction of O(^{1}D) with ethane and propane, as well as many other chemical reactions with deep wells in the interaction region. This study provides an excellent example of multiple dynamical pathways in a single chemical reaction, which opens enormous opportunities in theoretically investigating the dynamics of complicated chemical reactions which are important in combustion chemistry.

Acknowledgments

This work was supported by the National Natural Science Foundation of China (Grant Nos. 21303197 and 90921014), Ministry of Science and Technology of China (2013CB834601), and Youth Innovation Promotion Association (2015143), the Chinese Academy of Sciences.

[1] J. J. Lin, J. Zhou, W. Shiu and K. Liu, *Science*, 2003, **300**, 966.

[2] J. P. Camden, H. A. Bechtel, D. J. Ankeny Brown, M. R. Martin, R. N. Zare, W. Hu, G. Lendvay, D. Troy and G. C. Schatz, *J. Am. Chem. Soc.*, 2005, **127**, 11898.

[3] S. Yan, Y.-T. Wu, B. Zhang, X.-F. Yue and K. Liu, *Science*, 2007, **316**, 1723.

[4] W. Zhang, H. Kawamata and K. Liu, *Science*, 2009, **50**, 303.

[5] W. Zhang, Y. Zhou, G. Wu, Y. Lu, H. Pan, B. Fu, Q. Shuai, L. Liu, S. Liu, L. L. Zhang *et al.*, *Proc. Natl. Acad. Sci. U. S. A.*, 2010, **107**, 12782.

[6] G. Czakó and J. M. Bowman, *Science*, 2011, **334**, 343.

[7] G. Czakó and J. M. Bowman, *Proc. Natl. Acad. Sci. U. S. A.*, 2012, **109**, 7997.

[8] Z. Zhang, Y. Zhou, D. H. Zhang, G. Czako and J. M. Bowman, *J. Phys. Chem. Lett.*, 2012, **3**, 3416.

[9] R. Liu, M. Yang, G. Czak´, J. M. Bowman, J. Li and H. Guo, *J. Phys. Chem. Lett.*, 2012, **3**, 3776.

[10] R. Welsch and U. Manthe, *J. Phys. Chem. Lett.*, 2015, **6**, 338.

[11] J. W. Cao, Z. J. Zhang, C. F. Zhang, K. Liu, M. H. Wang and W. S. Bian, *Proc. Natl. Acad. Sci. U. S. A.*, 2009, **106**, 13180.

[12] B. Fu, Y. Han, J. M. Bowman, L. Angelucci, N. Balucani, F. Leonori and P. Casavecchia, *Proc. Natl. Acad. Sci. U. S. A.*, 2012, **109**, 9733.

[13] B. Fu, Y. Han, J. M. Bowman, F. Leonori, N. Balucani, L. Angelucci, A. Occhiogrosso, R. Petrucci and P. Casavecchia, *J. Chem. Phys.*, 2012, **137**, 22A532.

[14] J. Y. Yang, K. J. Shao, D. Zhang, Q. Shuai, B. Fu, D. H. Zhang and X. Yang, *J. Phys. Chem. Lett*, 2014, **5**, 3106.

[15] Y. Zhou, B. Fu, C. Wang, M. A. Collins and D. H. Zhang, *J. Chem. Phys.*, 2011, **134**, 064323.

[16] R. Welsch and U. Manthe, *J. Chem. Phys.*, 2014, **141**, 051102.

[17] J. Shu, J. J. Lin, C. C. Wang, L. Y. T. and X. Yang, *J. Chem. Phys.*, 2001, **115**, 842.

[18] J. J. Lin, J. Shu, Y. T. Lee and X. Yang, *J. Chem. Phys.*, 2000, **113**, 5287.

[19] X. Yang, *Phys. Chem. Chem. Phys.*, 2006, **8**, 205.

[20] J. Shu, J. J. Lin, Y. T. Lee and X. Yang, *J. Chem. Phys.*, 2001, **115**, 849.

[21] J. Shu, J. J. Lin, Y. T. Lee and X. Yang, *J. Chem. Phys.*, 2001, **114**, 4.

[22] J. Shu, J. J. Lin, Y. T. Lee and X. Yang, *J. Am. Chem. Soc.*, 2001, **123**, 322.

[23] C. C. Miller, R. van Zee and J. Stephenson, *J. Chem. Phys.*, 2000, **113**, 5287.

[24] H. Kohguchi, Y. Ogi and T. Suzuki, *Phys. Chem. Chem. Phys.*, 2008, **10**, 7222.

[25] H. Kohguchi, Y. Ogi and T. Suzuki, *Phys. Chem. Chem. Phys.*, 2011, **13**, 8371.

[26] Y. Ogi, H. Kohguchi and T. Suzuki, *Phys. Chem. Chem. Phys.*, 2013, **15**, 12946.

[27] Q. Shuai, H. Pan, J. Yang, D. Zhang, B. Jiang, D. Dai and X. Yang, *J. Phys. Chem. Letts.*, 2012, **3**, 1310.

[28] Q. Shuai, H. Pan, J. Yang, D. Zhang, B. Jiang, D. Dai and X. Yang, *J. Chem. Phys.*, 2012, **137**, 224301.

[29] M. González, J. Hernando, I. Baños and R. Sayós, *J. Chem. Phys.*, 1999, **111**, 8913.

[30] J. Hernando, J. Millán, R. Sayós and M. González, *J. Chem. Phys.*, 2003, **119**, 9504.

[31] R. Sayós, J. Hernando, M. P. Puyuelo, P. A. Enriquez and M. González, *Phys. Chem. Chem. Phys.*, 2002, **4**, 288.

[32] H. G. Yu and J. T. Muckerman, *J. Phys. Chem. A*, 2004, **108**, 8615.

[33] R. B. Bouchrit, M. Jorfi, D. B. Abdallah, N. Jaidane, M. González, B. Bussery-Honvault and P. Honvault, *J. Chem. Phys.*, 2014, **140**, 244315.

[34] X. Liu, J. J. Lin, S. Harich, G. C. Schatz and X. Yang, *Science*, 2000, **289**, 1536.

[35] H. Guo, *Int. Rev. Phys. Chem.*, 2012, **31**, 1.

[36] T. Martínez, M. L. Hernández, J. M. Alvariño, F. J. Aoiz and V. S. Rábanos, *J. Chem. Phys.*, 2003, **119**, 7871.

[37] P. G. Jambrina, I. Montero, F. J. Aoiz, J. Aldegunde and J. M. Alvariño, *Phys. Chem. Chem. Phys.*, 2012, **14**, 16338.

[38] B. J. Braams and J. M. Bowman, *Int. Rev. Phys. Chem.*, 2009, **28**, 577.

[39] J. M. Bowman, G. Czakó and B. Fu, *Phys. Chem. Chem. Phys.*, 2011, **13**, 8094.

[40] H. J. Werner *et al.*, *MOLPRO, version 2010.1, a package of ab initio programs, see details in http://www.molpro.net/*, 2010.

[41] M. P. Deskevich, D. J. Nesbitt and H. J. Werner, *J. Chem. Phys.*, 2004, **120**, 7281.

[42] K. P. Huber and G. Herzberg, *in NIST Chemistry WebBook, http://webbook.nist.gov.*

[43] J. Sun and K. Ruedenberg, *J. Chem. Phys.*, 1993, **99**, 5269.

[44] J. Chase, W. W., C. A. Davies, J. Downey, R., D. J. Frurip, R. A. McDonald and A. N. Syverud, *J. Phys. Chem. Ref. Data, Suppl. 1*, 1985, **14**, 1.

[45] W. L. Hase, *Classical Trajectory Simulations: Initial Conditions, a chapter in Encyclopedia of Computational Chemistry*, ed. N. L. Allinger, Wiley, New York, 1998, vol. 1, pp. 402–407.

[46] W. L. Hase, *Classical Trajectory Simulations: Final Conditions, a chapter in Encyclopedia of Computational Chemistry*, ed. N. L. Allinger, Wiley, New York, 1998, vol. 1, pp. 399–402.

[47] B. Fu, D. H. Zhang and J. M. Bowman, *J. Chem. Phys.*, 2013, **139**, 024303.

[48] G. Czakó and J. M. Bowman, *J. Chem. Phys.*, 2009, **131**, 244302.

[49] B. Fu, E. Kamarchik and J. M. Bowman, *J. Chem. Phys.*, 2010, **133**, 164306.

Caption of Figures:

Fig. 1 Schematic of the ground-state PES of the $O(^1D)+CH_4$ multichannel reaction. The reaction energetics of the $OH+CH_3$, the H formation, the H_2 formation and CH_2+H_2O channels are indicated by blue, green, purple, and red lines, respectively. The fitted energies are in kcal/mol, relative to the reactants $O(^1D)$ + CH_4, and those shown in parentheses are from MRCI+Q/aug-cc-pVTZ calculations. All of the energies are shown without vibrational zero-point energy correction.

Fig. 2 Minimum energy reaction paths of the $O(^1D)+CH_4$ multichannel reaction obtained from the PES (solid lines) and those calculated from MRCI+Q/aVTZ theory (symbols).

Fig. 3 (a) Center-of-mass (CM) translational energy distribution of OH + CH_3 obtained from the QCT calculations. The total available energy is indicated by black arrow. (b) Angular distribution of OH relative to the direction of the incoming $O(^1D)$.

Fig. 4 (a) Vibrational state distribution of OH for the OH + CH_3 channel . (b) Rovibrational state distributions of OH up to v=4.

Fig. 5 (a) Mode-specifc vibrational state distribution of CH_3 for the OH + CH_3 channel . (b) Rotational state distribution of CH_3.

Fig. 6 3D polar plot for the product translational energy and angular distributions for the $OH+CH_3$ channel. The forward direction (0°) corresponds to the direction of the $O(^1D)$ reagent.

Fig. 7 (a) Total translational energy distribution of the H formation channel (sum of contributions of $H+CH_2OH$ and $H+CH_3O$). The total available energies for each channel are indicated by black arrows. (b) Angular distribution of CH_2OH/CH_3O relative to the direction of the incoming $O(^1D)$.

Fig. 8 Same as Fig. 6 except for the H formation channel.

Fig. 9 (a) Total translational energy distribution of the H_2 formation channel, together with the translational energy distributions of H_2+HCOH and H_2+H_2CO pathways, respec-

tively. The total available energies for each channel are indicated by black arrows. (b) Angular distribution of HCOH/H_2CO relative to the direction of the incoming $O(^1D)$.

Fig. 10 Same as Fig. 6 except for the H_2 formation channel.

Fig. 11 The distributions of reaction time (fs) for trajectories of OH, H and H_2 formation channels.

TABLE I: Relative Energy (kcal/mol), Zero Point Energy (kcal/mol), and Harmonic Frequenceis (cm^{-1}) for the $O(^1D) + CH_4$ System

Species	Energy[a]	ZPE	Frequencies[b]
$O(^1D) + CH_4$	0.00(0.00)	28.87	1365(t), 1584(e), 3130, 3196(t)
			[1306(t), 1534(e), 2917, 3016(t)]
$OH + CH_3$	−39.68(−39.42)	24.68	3804; 514, 1467(e), 3109, 3346(e)
			[3738; 603, 1403(e), 3004, 3171(e)]
$H + CH_2OH$	−31.50(−31.47)	23.69	405, 474, 1074, 1260, 1436, 1532,
			3211, 3313, 3910
			[420, 482, 1048, 1183, 1334, 1459,
			3043, 3162, 3674]
$H + CH_3O$	−23.23(−23.67)	22.85	826(e), 1040, 1392, 1479(e), 2948, 2985(e)
			[652(e), 1044, 1376, 1412(e), 2840, 2955(e)]
$H_2 + H_2CO$	−106.00(−106.02)	23.41	4515; 1159, 1313, 1574, 1782, 2959(e)
			[4401; 1167, 1249, 1500, 1746, 2783(e)]
H_2 + *cis*-HCOH	−48.57(−48.35)	23.18	4341; 1184, 1319, 1386, 1606, 2690, 3692
H_2 + *trans*-HCOH	−53.66(−53.22)	23.94	4294; 1193, 1273, 1360, 1691, 2835, 3890
$H_2O + CH_2$	−37.37(−37.33)	24.54	1409, 2877, 2972; 1720, 3940, 3964
TS1	−37.66(−37.77)	28.24	2138*i*, 869, 1128, 1158, 1309, 1394, 1530,
			1680, 1884, 2872, 2913, 3020
cis-TS2	−39.18(−38.87)	26.58	921*i*, 646, 722, 1056, 1155, 1268, 1357,
			1501, 1680, 2839, 2856, 3512
trans-TS2	−42.27(−41.95)	26.56	985*i*, 546, 704, 922, 1149, 1214, 1438,
			1521, 1614, 2635, 3034, 3803
TS3	−47.14(−46.64)	28.66	847*i*, 434, 539, 832, 1119, 1302, 1422, 1620,
			2730, 2996, 3083, 3971
vdw	−49.78(−49.69)	30.24	261, 365, 485, 627, 1165, 1300, 1459, 1841,
			2861, 2883, 3782, 4083
CH_3OH	−135.88(−135.99)	32.03	238, 1015, 1047, 1181, 1454, 1460, 1485,
			1525, 2998, 3079, 3124, 3796
			[200, 1033, 1060, 1165, 1345, 1455, 1477,
		20	1477, 2844, 2960, 3000, 3681]

[a] The fitted energies are relative to $O(^1D) + CH_4$. The values in the parentheses are from MRCI+Q/aug-cc-pVTZ calculations relative to $O(^1D) + CH_4$. [b] The available experimental values[42] are shown in the brackets.

TABLE II: Comparison between theoretical[a] and experimental (0 K) energetics for the $O(^1D)$+CH_4 reaction

Species	Theory	Experiment(Ref. [44])
$O(^1D) + CH_4$	0.0	0.0
$OH + CH_3$	−43.8	-43.6
$H + CH_2OH$	−36.7	-39.5
$H + CH_3O$	−29.3	-30.9
$H_2 + H_2CO$	−111.5	-115.3
H_2 + *trans*-HCOH	−58.6	-61.0
$H_2O + CH_2$	−41.7	-42.8
CH_3OH	−132.72	-133.7

[a] Energies in kcal/mol include the zero-point energy.

TABLE III: Comparison between theoretical and experimental branching ratios of product channels at E_c=6.8 kcal/mol for the $O(^1D) + CH_4$ reaction

Product Channel	Theory	Experiment(Ref. [18])
$OH+CH_3$	84.2%	77%
$H+CH_2OH/CH_3O$	12.2%	18%
H_2+HCOH/H_2CO	3.6%	5%